THE PROTEIN SOCIETY

Concerted millisecond timescale dynamics in the intrinsically disordered carboxyl terminus of γ-tubulin induced by mutation of a conserved tyrosine residue

Jason Harris,[1] Maria Shadrina ,[2] Carlos Oliver,[2,3] Jackie Vogel,[2,3]* and Anthony Mittermaier[1]*

[1]Department of Chemistry, McGill University, 801 Sherbrooke St. W, Montreal, Quebec, Canada
[2]Department of Biology, McGill University, 3649 Promenade Sir William Osler, Montreal, Quebec, Canada
[3]The School of Computer Science, McGill University, 3480 University St, Montreal, Quebec, Canada

Received 5 September 2017; Accepted 7 November 2017
DOI: 10.1002/pro.3345
Published online 11 November 2017 proteinscience.org

Abstract: Tubulins are an ancient family of eukaryotic proteins characterized by an amino-terminal globular domain and disordered carboxyl terminus. These carboxyl termini play important roles in modulating the behavior of microtubules in living cells. However, the atomic-level basis of their function is not well understood. These regions contain multiple acidic residues and their overall charges are modulated in vivo by post-translational modifications, for example, phosphorylation. In this study, we describe an application of NMR and computer Monte Carlo simulations to investigate how the modification of local charge alters the conformational sampling of the γ-tubulin carboxyl terminus. We compared the dynamics of two 39-residue polypeptides corresponding to the carboxyl-terminus of yeast γ-tubulin. One polypeptide comprised the wild-type amino acid sequence while the second contained a Y > D mutation at Y11 in the polypeptide (Y445 in the full protein). This mutation introduces additional negative charge at a site that is phosphorylated in vivo and produces a phenotype with perturbed microtubule function. NMR relaxation measurements show that the Y11D mutation produces dramatic changes in the millisecond-timescale motions of the entire polypeptide. This observation is supported by Monte Carlo simulations that—similar to NMR—predict the WT γ-CT is largely unstructured and that the substitution of Tyr 11 with Asp causes the sampling of extended conformations that are unique to the Y11D polypeptide.

Keywords: γ-tubulin; intrinsically disordered proteins; NMR relaxation; Monte Carlo simulations; polypeptide conformational ensembles; disorder-to-disorder transition

Additional Supporting Information may be found in the online version of this article.

Jason Harris and Maria Shadrina contributed equally to this study

Grant sponsor: CDMC-CREATE graduate fellowship from Natural Sciences and Engineering Research Council of Canada; Grant number: 327028-09 (C.O.); Grant sponsor: Hydro Quebec fellowship (J.H.); Grant sponsor: Canadian Institutes of Health Research; Grant number: MOP-123335 (J.V.); Grant sponsor: Natural Sciences and Engineering research Council of Canada; Grant number: 327028-09 (A.M.).

*Correspondence to: Anthony Mittermaier, Department of Chemistry, McGill University, 801 Sherbrooke St. W, Room 102, Montreal, QC, Canada. E-mail: anthony.mittermaier@mcgill.ca or Jackie Vogel, Department of Biology, McGill University, 3649 Promenade Sir William Osler, Room 269, Montreal, QC, Canada. E-mail: jackie.vogel@mcgill.ca

Introduction

Tubulins comprise an ancient and evolutionarily conserved family of globular proteins found in all eukaryotic cells. α- and β-tubulins associate as heterodimers and assemble into highly dynamic microtubule biopolymers, while the dominant pathway for the nucleation of the microtubule polymer is promoted by γ-tubulin. Together, α-, β-, and γ-tubulins coordinate the dynamical properties and plastic organization of microtubules, giving rise to cell shape and orchestrating the segregation of chromosomes during cell division. High-resolution crystal structures of members of the tubulin family (α-, β-, and γ-tubulins) revealed that tubulins consist of an evolutionarily conserved globular domain[1,2] and an acidic, solvent-accessible and generally disordered carboxyl terminus (CT) whose length varies across members of the tubulin family. Regions within the globular domain, for example, those involved in GTP binding and interaction surfaces responsible for dimerization and polymerization are some of the most conserved among all eukaryotic proteins. In contrast, the primary amino acid sequences of α-, β-, and γ-tubulin CTs are generally divergent, yet all contain clusters of Glu and Asp residues. These negatively charged clusters are particularly prominent in the CTs of α- and β-tubulin (α-CTs and β-CTs), which are frequently referred to as "E-hooks" as they are thought to project outward from the microtubule lattice and interact with the local environment.

The biological function of α-CTs and β-CTs has been strongly linked to the electrostatic interactions between the negatively charged "E-hook" and the surface of the α,β-heterodimers and with microtubule associating proteins (MAPs) such as the molecular motors kinesin and dynein and other proteins that modulate the dynamical properties of microtubules. Residues in the CTs of α- and β-tubulins are targeted for a large number of post-translational modifications (PTMs) including tyrosinylation, glutamylation, and phosphorylation.[3] The diversity of known modifications to the CTs of α- and β-tubulins is viewed as a large and complex "tubulin code" for which the functional significance and biophysical mechanisms are only now emerging.[4] However it appears that a combination of sequence diversity, specific motifs, and PTMs all contribute to how α- and β-CTs control their interaction with molecular motors and MAPs that expand the functional repertoire of microtubules.[5]

The biological function of the γ-tubulin CT is far less understood than for α- or β-tubulins. Similar to the α-CT and β-CT, the length of the γ-CT varies between organisms and it is characterized by sequence diversity and structural disorder. Few PTMs have been identified for γ-CTs. One exception is the in vivo phosphorylation of an evolutionarily conserved Tyr residue in the γ-tubulin orthologue of the budding yeast *Saccharomyces cerevisiae* (Y443 in human, Y445 in yeast; S.c.).[6,7] Mutation of Y445 to an acidic residue (Asp or Glu) alters microtubule dynamics and perturbs the function of the mitotic spindle but does not appear to alter microtubule nucleation,[6] suggesting the S.c. γ-CT may function in postnucleation organization and function of microtubules. This Tyr residue together with the hydrophobic residues at positions +1 and +2 are invariant across γ-tubulins from fungi, animals, and plants,[7] suggesting that this aspect of γ-CT regulation is also evolutionarily conserved.

Despite their functional significance, little is known regarding the structure and dynamics of the CTs of α-, β-, and γ-tubulins, as their conformational flexibility makes them difficult to study by X-ray crystallography or electron microscopy. The structures of a mammalian α,β-tubulin dimer and human γ-tubulin have been solved by X-ray crystallography.[1,2] However, flexible regions including loops and the 35 residues C-terminal to the end of helix 12 (i.e., γ-CT) were not visualized. Our understanding of the dynamic structure of tubulin CTs is currently based on molecular dynamics simulations of the β-tubulin CT which focused on conformational sampling[8] and interactions between CT residues and residues in the globular domain located at the microtubule surface.[9] To date, the conformational sampling and biophysical properties of tubulin CTs have not been investigated experimentally.

A combination of Nuclear Magnetic Resonance (NMR) spectroscopy and Monte Carlo (MC) computer simulations are ideally suited for characterizing the structural and dynamical properties of the γ-CT. This combination of techniques has been previously applied to intrinsically disordered proteins, providing detailed atomic resolution insight into the relationship between conformational sampling and biological function.[10] We used NMR spectroscopy and MC simulations to study the last 39 residues of yeast γ-tubulin, both of the wild-type (WT) and the previously characterized Y > D mutation.[6] Surprisingly, we find that the Tyr to Asp substitution (Y445D full-length, Y11D γ-CT) induces globally concerted dynamics occurring on the millisecond timescale. This is likely due to additional electrostatic repulsion involving D11. We hypothesize that the negative charge accompanying phosphorylation of this tyrosine has a similar effect as the Y > D mutation, potentially modulating the accessibility of the γ-CT for interactions with binding partners. To our knowledge, such cooperative transitions occurring exclusively between unfolded sub-populations have not been previously reported, and represent a novel way to regulate the function of intrinsically disordered protein domains.

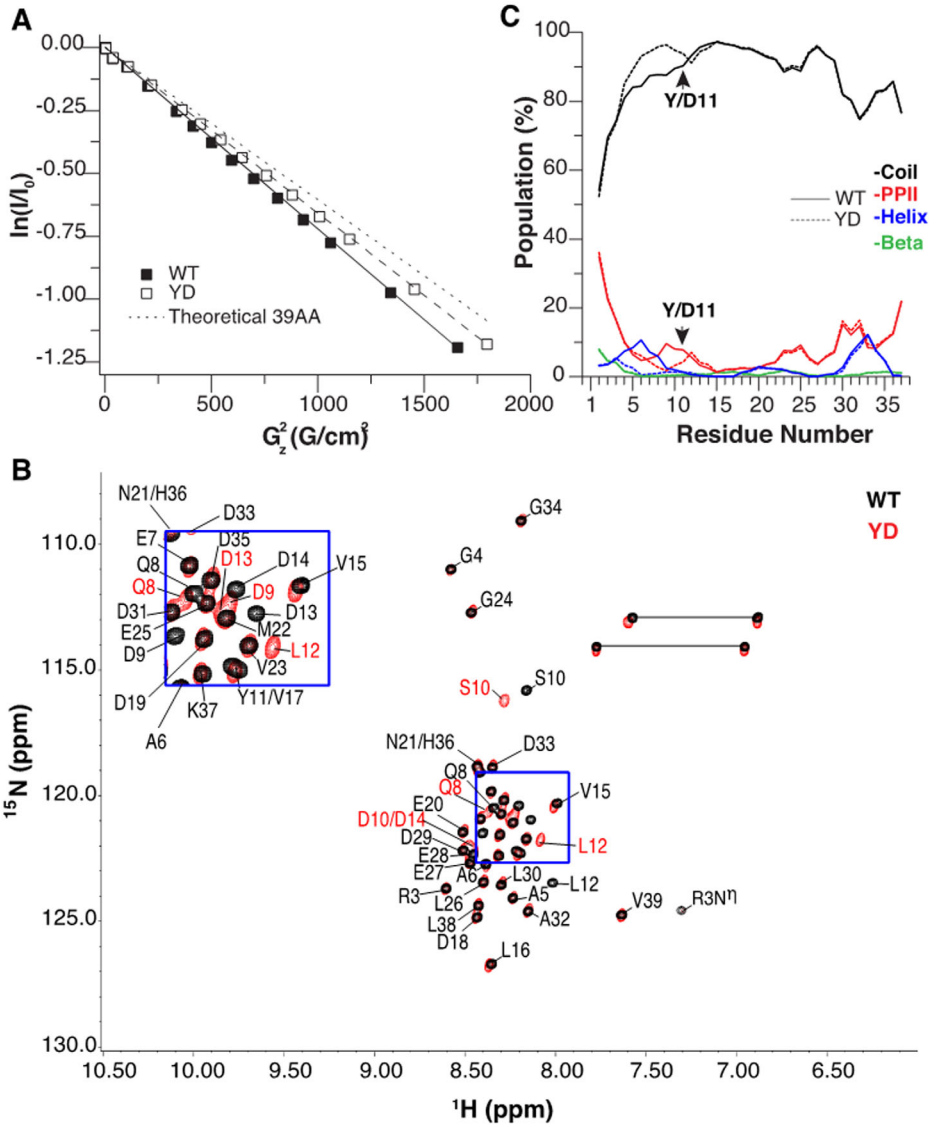

Figure 1. NMR data for the γ-tubulin CT. (A) NMR gradient diffusion data. The natural logarithms of normalized ^{1}H methyl peak intensities (ln{I/I_0}) are plotted as a function of the square of the strength of the magnetic field gradient (G_z^2) applied during a diffusion delay for WT (filled squares) and Y11D (hollow squares) γ-CT polypeptides. The slopes (solid lines) are proportional to the translational diffusion constants. Experimental uncertainties are smaller than the symbols used. The dashed line corresponds to the expected ln{I/I_0} versus G_z^2 relationship for a typical random coil polypeptide of 39 amino acids.[12] (B) ^{1}H–^{15}N correlation spectra of WT (black) and Y11D (red) γ-CT polypeptides. The blue inset shows an enlargement of the central region. Residue-specific assignments are indicated for each peak. Black labels correspond to the WT and overlaying Y11D peaks. Assignments of perturbed Y11D peaks are indicated in red. (C) Secondary structure content determined from backbone NMR chemical shifts using δ2D software[19] plotted as a function of residue number for WT (solid line) and Y11D γ-CT (dashed line) polypeptides with black, blue, green, and red indicating the percentage of random coil, α-helical, β-sheet, and poly-proline II helical conformations, respectively.

Results

Hydrodynamic radii of the WT and Y11D γ-CT polypeptides

We used NMR pulsed field gradient diffusion experiments[11] to determine the effective hydrodynamic radii of the WT and Y11D γ-CT polypeptides. Figure 1(A) shows the peak intensities of well-resolved up-field methyl ^{1}H peaks, plotted as a function of the square of the magnetic field gradient strength. The slopes of the fitted lines give the translational diffusion coefficients (D_s, see Methods section). The diffusion coefficient thus obtained for the WT γ-CT polypeptide ($D_s = 1.25 \pm 0.01 \times 10^{-6}$ cm^2/s) was significantly larger than that of the Y11D γ-CT polypeptide ($D_s = 1.15 \pm 0.01 \times 10^{-6}$ cm^2/s, $p < 1 \times 10^{-5}$). We calculated the effective hydrodynamic radii of the γ-CT polypeptides using the Stokes–Einstein equation:

$$D_s = \frac{k_B T}{6\pi\eta r} \quad (1)$$

where D_s is the experimentally determined diffusion coefficient, k_B is the Boltzmann constant, T is the

temperature in degrees Kelvin, η is the viscosity of the medium, and r is the Stokes radius of the molecule. We obtained effective hydrodynamic radii of 14.2 ± 0.2 Å for the WT γ-CT polypeptide and 15.6 ± 0.2Å for the Y11D γ-CT polypeptide. We compared these values to those found for library of denatured proteins in which the logarithm of the Stokes radius was found to depend linearly on logarithm of the number of residues such that[12]

$$r = 2.518N^{0.522} \quad (2)$$

where N is the number or residues. This empirical relationship predicts that 39-residue denatured polypeptides have Stokes radii of 17 Å, that is, more expanded than what we observe for either γ-CT. Notably, the 39-residue WT γ-CT has an even smaller Stokes radius ($r = 14.2$ Å) than the 32-residue fibronectin binding protein D3 in 8M urea ($r = 14.9$ Å).[13]

Chemical shift-based secondary structure predictions

^{1}H–^{15}N HSQC correlation spectra of the WT and Y11D γ-CT polypeptides are shown in Figure 1(B). The lack of dispersion in the ^{1}H dimension is characteristic of unstructured polypeptide chains, as expected.[14] We assigned 38 ^{1}H–^{15}N correlations to 38 of 39 residues for both molecules using a combination of HNCA, HNCO,[15] HNCACB,[16] CBCA(CO)NH,[17] C(CO)NH,[18] and HCCONH[18] experiments. The largest differences in chemical shift between the WT and Y11D γ-CT polypeptides were observed for residues surrounding the Y11D mutation site [Q442, D443, S444, L446, D447, and D448, Fig. 1(B), inset]. NMR data for the two polypeptide chains were analyzed using δ2D software,[19] which compares the experimental backbone chemical shifts to those expected for different types of protein secondary structure. Predictions for the most populated secondary structure have been found to be accurate to within 10%, and differences between two related samples are within 2%.[19] According to the δ2D predictions [Fig. 1(C)], the WT and Y11D γ-CT polypeptides are predominantly random coils with regions of weak (5–10%) α-helical and β-sheet propensity. The percentage of random coil character increases from about 88% in the WT γ-CT polypeptide to about 96% in the Y11D γ-CT polypeptide for residues near Y11D, suggesting that the Y > D mutation leads to a modest local increase in flexibility.

Nanosecond–picosecond dynamics γ-CT polypeptides

We characterized the dynamics of the WT and Y11D γ-CT polypeptides using ^{15}N spin relaxation NMR experiments. Initially, we measured longitudinal relaxation rates (R_1),[20] transverse relaxation rates (R_2),[21] and steady-state ^{1}H–^{15}N heteronuclear NOE (hnNOE) values.[21] The R_1, R_2, and hnNOE measurements are sensitive to motions on the nanosecond to picosecond timescales. R_2 relaxation rates are additionally influenced by dynamics on the millisecond to microsecond timescales. As seen in Figure 2(A,B), the values of R_1 and hnNOE obtained for the WT and Y11D polypeptides are nearly identical, suggesting that the mutation does not significantly affect motions of the backbone on the nanosecond to picosecond timescales. In contrast, R_2 values for the Y11D γ-CT polypeptide are significantly larger than those of the WT [Fig. 2(C)]. These differences could be attributed to motions on the microsecond to millisecond timescales that lead to peak broadening and elevated transverse relaxation rates.[22] To test this hypothesis, we performed additional $R_{1\rho}$ transverse

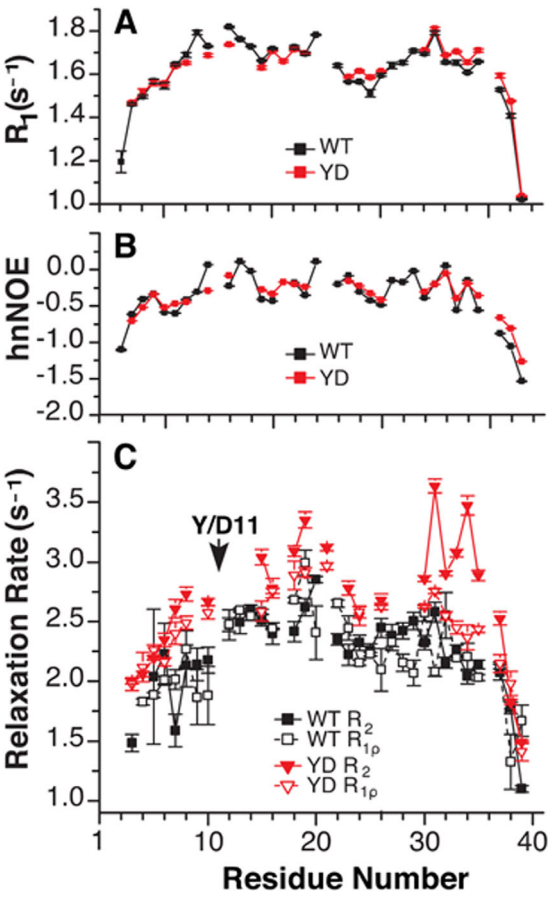

Figure 2. Experimental ^{15}N NMR spin relaxation parameters plotted as a function of residue number for WT (black squares) and Y11D (red triangles) γ-CT polypeptides for (A) longitudinal and (B) transverse ^{15}N spin relaxation rates (R_1 and R_2, $R_{1\rho}$) and (C) steady-state heteronuclear NOE (hnNOE) data. In C, ^{15}N transverse relaxation rates obtained with refocusing pulses applied during the relaxation delay (R_2) are indicated with solid symbols while those obtained with a ^{15}N spin-lock applied during the relaxation delay ($R_{1\rho}$) are indicated with hollow symbols. Gaps in the data are due to overlap in the ^{1}H–^{15}N correlation spectra.

relaxation experiments. The $R_{1\rho}$ and R_2 are experiments essentially identical with the one major difference that, during the relaxation delay, the R_2 pulse sequence applies a train of refocusing pulses while the $R_{1\rho}$ pulse sequence applies a spin-lock. The spin-lock is more efficient at quenching dynamical broadening under our experimental conditions, therefore if broadening contributes to the observed R_2 values, we would expect to observe $R_{1\rho} < R_2$. As seen in Figure 2(C), the $R_{1\rho}$ values are much lower than R_2 values for the Y11D γ-CT polypeptide while $R_{1\rho} \approx R_2$ for the WT γ-CT. Furthermore, the $R_{1\rho}$ values of the Y11D γ-CT polypeptide approach the R_2 and $R_{1\rho}$ values obtained for the WT γ-CT. This strongly suggests that the Y11D γ-CT polypeptide undergoes motions on the microsecond to millisecond timescale that are absent in the WT γ-CT polypeptide.

Microsecond–picosecond dynamics of γ-CT polypeptides

To gain further insight into the microsecond to millisecond timescale dynamics produced by the Y > D mutation, we performed the Carr–Purcell–Meiboom–Gill (CPMG) relaxation dispersion experiments[23] on the WT and Y11D γ-CT polypeptides using an 18.8 T (800 MHz) NMR spectrometer. Exchange among different conformational states can produce fluctuations in chemical shifts that lead to spectral broadening and elevated transverse relaxation rates (R_2). In a CPMG experiment, this dynamical broadening is quenched by applying variable numbers of 180° refocusing pulses during a constant relaxation delay. As the pulse repetition rate (ν_{CPMG}) increases, the broadening due to microsecond–millisecond dynamics is reduced leading to lower transverse relaxation rates. R_2 versus ν_{CPMG} plots for the Y11D γ-CT polypeptide exhibit decreasing profiles that are characteristic of dynamical broadening [Fig. 3(A)]. In contrast, dispersion profiles for the WT γ-CT are flat, suggesting that this polypeptide does not undergo microsecond-millisecond timescale dynamics. The broadening exhibited by the Y11D γ-CT polypeptide could be due to intra-molecular conformational exchange, intermolecular association/dissociation, or a combination of the two. In order to discriminate between these possibilities, the Y11D γ-CT sample was diluted twofold and the CPMG experiment was repeated. The shapes and magnitudes of the dispersion curves were not affected by dilution [Fig. 3(A)], indicating that the spectral broadening exhibited by the Y11D γ-CT polypeptide is due to conformational exchange not intermolecular self-association.

CPMG data can be analyzed to yield quantitative information on the underlying molecular motions. For instance, if it is assumed that the spectral broadening is due to dynamical exchange between two different conformations, CPMG data

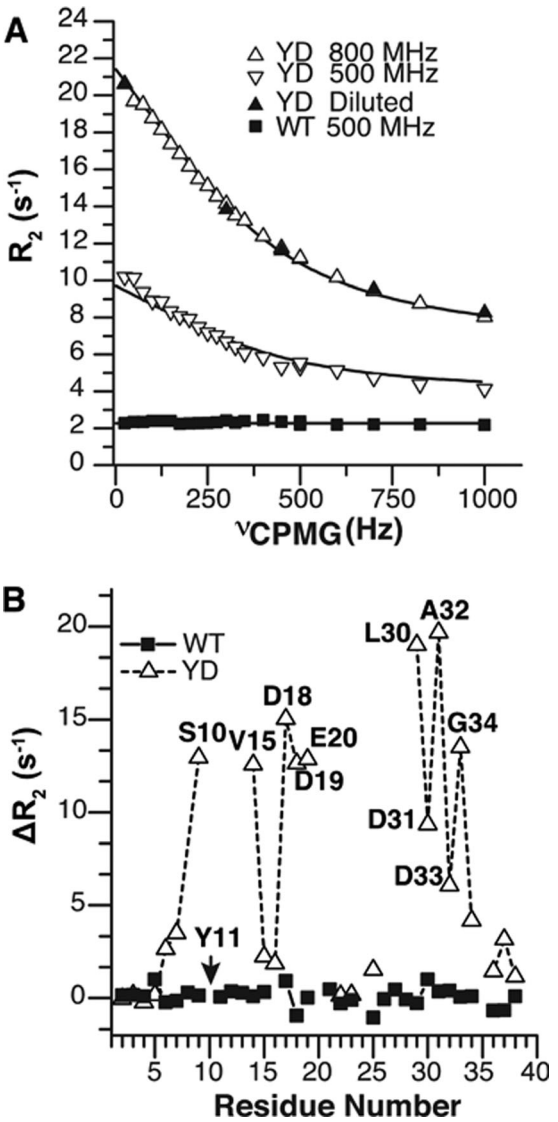

Figure 3. NMR CPMG relaxation dispersion data. (A) ^{15}N CPMG profiles for Val 15 (449 in the full-length protein) of WT (filled squares) and Y11D (hollow triangles) γ-CT polypeptides. Data for a 50%-diluted Y11D sample are shown with filled triangles, aligned along the vertical axis to superpose the 25 Hz ν_{CPMG} data points. Solid curves correspond to the best fit to a dynamical model comprising concerted exchange between two conformational states. (B) Magnitudes of ^{15}N relaxation dispersion profiles, $\Delta R_2 = R_2(\nu_{CPMG} = 25\ Hz) - R_2(\nu_{CPMG} = 1000\ Hz)$, plotted as a function of residue number for WT (squares) and Y11D (triangles) γ-CT polypeptides. Gaps in the data are due to overlap in ^1H–^{15}N correlation NMR spectra.

can be fit to a model that yields the populations of the two states (p_A and p_B), the exchange rate ($k_{ex} = k_{AB} + k_{BA}$), and the difference in the resonance frequencies of the two states ($\Delta\omega$).[22] To obtain reliable exchange parameters, it is preferable to acquire CPMG data at two different static magnetic fields, as the magnetic field dependence of dynamical broadening is closely related to the timescale of the dynamics.[24] We therefore repeated the CPMG experiments at 11.7 T (500 MHz). In this case, the

magnitudes of the dispersions were ~1.5-fold smaller at 500 MHz compared to 800 MHz [Fig. 3(A)]. This is consistent with dynamics on the intermediate timescale regime with $k_{ex} \approx \Delta\omega$.[25] We fit all dispersion profiles to a two-state exchange model (see Methods). The extracted values of k_{ex} and p_B were similar for all dispersions, which suggested that all the nuclei might be sensing the same global exchange process (data not shown). We therefore repeated the analysis fitting all dispersion profiles with identical (global) values of p_B and k_{ex}, and optimizing $\Delta\omega$ on a per-residue basis. Excellent agreement was obtained for all residues [Fig. 3(A) and Supporting Information, Fig. S1], implying that the CPMG data are consistent with concerted motions involving the entire γ-CT polypeptide chain. In other words, the Y11D γ-CT polypeptide populates two distinct states, a major form populated to about 97.5% and a minor form populated to about 2.5%, which exchange with a rate of 2252 s^{-1}. Residues that show large dispersions have different chemical shifts in the two states, while residues in the Y11D γ-CT polypeptide that have smaller or flat dispersions have similar chemical shifts in the two states and are less affected by the conformational exchange process. Interestingly, the residues with the largest dispersions, that is, those whose local environments are most affected by conformational exchange, are located throughout the Y11D γ-CT polypeptide, up to 23 amino acids distant from the site of the D11 mutation. Figure 3(B) shows dispersion magnitude ($\Delta R_2 = R_2(\nu_{CPMG} = 25\ Hz) - R_2(\nu_{CPMG} = 1000\ Hz)$) plotted as a function of residue number for both WT and Y11D polypeptides. The WT γ-CT yielded $\Delta R_2 \approx 0$ throughout the length of the polypeptide, consistent a complete absence of millisecond to microsecond timescale motions. The Y11D γ-CT polypeptide contains multiple residues with large relaxation dispersions, as indicated by large values of ΔR_2. These predominantly fall into two clusters, the first located close to the mutation site (S10, V15, D18, D19, and E20) and the second involving several hydrophobic residues (L30, A32, and G34), which are located within a larger cluster of hydrophobic residues near the C-terminus [Fig. 3(B)]. Thus, a single Y > D substitution produces large concerted motions of the γ-CT involving dozens of residues, despite the observation that the ground state is almost entirely in a random coil state, according to backbone chemical shifts.

Monte Carlo (MC) simulations of conformational ensembles of the WT and Y11D γ-CTs

Our NMR experiments revealed that the Y11D γ-CT polypeptide populates two distinct states, which exchange on millisecond timescale. While the major state of Y11D (97.5%) behaves similarly to WT, the minor state of Y11D (2.5%) structurally differs from both major states (WT and Y11D). To provide structural insight into the observed difference between the γ-CTs, we performed MC simulations of the WT and Y11D variants. Since both polypeptides are highly negatively charged, the pK_a of the sidechain group of His 36 is expected to be larger than those of His residues in neutral peptides (up to ~7.1 from 6.0, unpublished results), which significantly increases the fraction of protonated His 36 (HisH+) in the population. Therefore, we simulated conformational ensembles of both WT and Y11D γ-CTs with neutral or charged His 36 (Supporting Information, Fig. S2). Based on 1,200,000 conformations sampled for each γ-CT variant, we plotted distributions of radii of gyration (R_g) for WT versus Y11D and WT HisH+ versus Y11D HisH+ [Fig. 4(A,B)]. Interestingly, when His 36 is taken to be neutral, the shapes of R_g distributions are similar for WT and Y11D with median R_g values of 14.7 and 14.8 Å, respectively. Protonation of His 36 results in higher population of extended conformations for Y11D HisH+ compared to WT HisH+. As a result, the median R_g value for Y11D HisH+ increases to 15.1 Å while the median R_g value of 14.7 Å remains for WT HisH+.

We calculated average diffusion coefficients for the sampled conformational ensembles of the four γ-CT variants: $D_s = 1.21 \times 10^{-6}$ cm^2/s for WT, Y11D, and WT HisH+, and 1.2×10^{-6} cm^2/s for Y11D HisH+. NMR diffusion measurements indicate that the average diffusion coefficients of the WT and Y11D γ-CTs are 1.25×10^{-6} and 1.15×10^{-6} cm^2/s, respectively, which are in a good agreement with their theoretical values, considering an expected range of error of $(0.02–0.12) \times 10^{-6}$ cm^2/s.[26] The smaller NMR-derived diffusion coefficient for the Y11D γ-CT polypeptide is consistent with its accessing more extended states that diffuse more slowly in solution. The MC simulations similarly show an expansion of the Y11D HisH+ relative to the WT [Fig. 4(B)] but interestingly not for the species containing a neutral His residue [Fig. 4(A)].

We also determined secondary structure content of the WT, Y11D, WT HisH+, and Y11D HisH+ ensembles based on backbone Φ/Ψ angles (Supporting Information, Fig. S3). In agreement with the experimental analysis of secondary structure [Fig. 1(C)], all four γ-CTs are mostly disordered with percentages of random coil of 82–83% and weak α-helical and β-sheet propensities corresponding to only 2–5%. The PPII population is more prominent than α-helical and β-sheet content and reaches 10–11% according to both MC and experimental results [Supporting Information, Fig. S3 vs Fig. 1(C)]. In summary, we found that WT, Y11D, WT HisH+, and Y11D HisH+ adopt similar conformational ensembles with a larger fraction of extended conformations in Y11D HisH+, which correlates with our experimental observations.

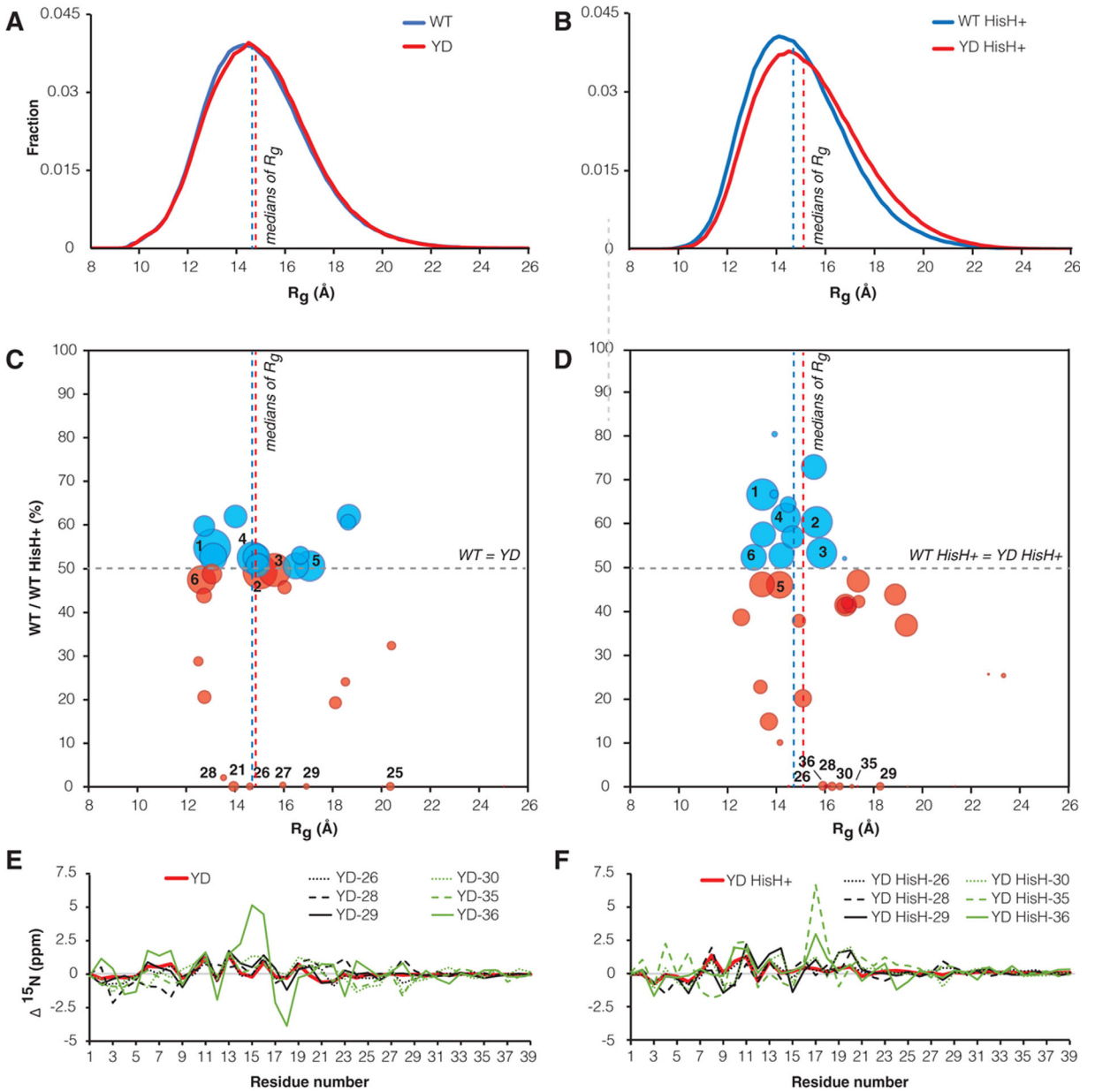

Figure 4. Monte Carlo simulation results for the WT vs Y11D γ-CT polypeptide (left panels) and the WT HisH+ vs Y11D HisH+ γ-CT polypeptide (right panels). (A,B) Histograms of radius of gyration (R_g) calculated for the conformational ensembles of the four γ-CT variants. The histograms of the wild-type and mutant variants are shown as blue and red lines, respectively. (C,D) Cluster distributions calculated based on the simulated polypeptide conformations. Cluster analyses were performed on the joined WT plus Y11D and WT HisH+ plus Y11D HisH+ ensembles. Clusters are shown as circles with a radius corresponding to cluster size (i.e., number of conformations) and plotted as a function of percentages of the WT/WT HisH+ conformations in a cluster vs average R_g of the cluster. Clusters, which include >50% of WT or WT HisH+ conformations, are colored in blue, clusters with <50% of WT or WT HisH+ are colored in red. The six largest clusters and clusters, which are unique for the mutant variants, are labeled for convenience. Full lists of clusters with % of the WT and mutant variants and average R_g values are provided in Supporting Information, Tables S1 and S2. (E,F) Relative theoretical ^{15}N chemical shifts of the mutant ensembles and clusters plotted as a function of residue number. Differences in the theoretical chemical shifts between the Y11D and WT ensembles and between the Y11D HisH+ and WT HisH+ ensembles are shown as red lines. Differences in the theoretical chemical shifts between the unique mutant clusters and corresponding wild-type ensembles are shown as black and green lines. The median R_g values indicated as dashed lines in panels A–D are 14.7, 14.8, 14.7, and 15.1 Å for the WT, Y11D, WT HisH+, and Y11D HisH+ ensembles, respectively.

Cluster analysis of conformational ensembles sampled for the WT and Y11D γ-CTs

The minor state of the Y11D γ-CT detected by NMR is populated to only 2.5% and hence it is masked in the MC simulations by conformations corresponding to highly populated major state, which represent the overwhelming majority of the ensemble. To identify conformers that are good candidates for the minor

state of Y11D, we performed cluster analysis on the joined ensembles of WT plus Y11D and WT HisH+ plus Y11D HisH+. Combining the wild-type and mutant ensembles allowed us to distinguish conformations that were sampled preferentially or exclusively by the Y11D or Y11D HisH+ γ-CTs. Only the C^{α} atoms were included in the cluster analysis. In total, 32 and 42 clusters were distinguished for the γ-CTs with neutral and protonated forms of His 36, respectively (Supporting Information, Tables S1 and S2). Supporting Information, Figures S4(A) and S5(A) illustrate polypeptide conformations in the six largest clusters for the both forms of His 36. We calculated average R_g and percentage of wild-type conformations for each cluster (Supporting Information, Tables S1 and S2) and plotted the cluster analysis data as scatter plots [Fig. 4(C,D)].

The largest clusters consist of 40–60% WT and 60–40% Y11D conformers for neutral His 36 and of 30–70% WT HisH+ and 70–30% Y11D HisH+ conformers for protonated His 36. In other words, most of the conformations sampled by the WT and Y11D polypeptides are structurally similar and fall into these large clusters. Notably, several smaller clusters contain 100% Y11D/Y11D HisH+ conformers (21, 25, 26, 27, 28, and 29 for Y11D, and 26, 28, 29, 30, 35, and 36 for Y11D HisH+). Therefore, they consist of conformations sampled exclusively by the mutant, corresponding to 4.5 and 4.0% of the entire Y11D and Y11D HisH+ ensembles, respectively. Supporting Information, Figures S4(B) and S5(B) show polypeptide conformations in the clusters observed only in the mutants for each protonated state of His 36. In the case of Y11D HisH+ (but not Y11D) many of these unique clusters have expanded radii of gyration, consistent with the overall expansion of the Y11D HisH+ ensemble seen in Figure 4(B). Interestingly, there are no clusters sampled by the WT that are not also well sampled by the mutant. In other words, the Y11D substitutions causes the γ-CT to broaden its overall conformational sampling to include new conformations not adopted by the WT with a concomitant expansion of the hydrodynamic radius.

Both the MC simulations and CPMG experiments detected minor (<5%) states populated exclusively by the Y11D γ-CT. In the case of NMR, the pervasive spectral broadening indicates that the local environments of residues throughout the polypeptide chain are affected by excursions to the minor state. To test whether the same is true for the MC-derived minor state(s), we estimated the average backbone ^{15}N chemical shifts for all conformers subjected to cluster analysis. Differences between the mean chemical shifts of the WT and Y11D polypeptides and the WT HisH+ and Y11D HisH+ polypeptides, averaging over all conformers, showed the largest changes in local environments of residues 3–22 [Fig. 4(E,F)], which correspond to the more compact N-terminus region of the polypeptides (Supporting Information, Figs. S4 and S5), in agreement with the NMR results. Interestingly, average ^{15}N chemical shifts of the unique Y11D/Y11D HisH+ clusters differ from the overall ensemble averages over the entire length of the sequence [Fig. 4(E,F)]. Thus, rare excursions to these clusters would be expected to modulate the chemical shifts of residues far from the site of the Y > D mutation, as seen by NMR.

Discussion

We performed a combination of NMR experiments and computer simulations to investigate the structural and dynamical consequences of introducing negative charge at a site in the γ-tubulin CT that is phosphorylated in vivo. The results derived from the two techniques were remarkably similar. Both showed that the WT γ-CT is largely unstructured, and that the substitution of Tyr 11 (Y445 in the full-length protein) with Asp leads to an increased fraction of extended conformations. The Y > D substitution causes pervasive dynamical broadening in NMR spectra that agrees quantitatively with a model in which the entire polypeptide chain undergoes transient excursions on the millisecond timescale to a set of rare conformations that are populated to about 2.5%. The WT does not exhibit these millisecond timescale motions. Similarly, the MC cluster analysis predicts that the Y > D substitution causes the γ-CT to adopt unique conformations that are not populated by the WT [Fig. 4(C,D)]. Most of these clusters have radii of gyration greater than the median, consistent with increased intramolecular electrostatic repulsion due to the introduction of additional negative charge to an already negatively charged molecule. Interestingly, the fraction of Y11D chains in these "unique" clusters is about 4%, while the fraction of chains in conformations similar to those adopted by the WT is 96%, on the same order as the populations of the excited and ground states determined by NMR. The MC simulations do not provide information on the heights of barriers and therefore do not make predictions regarding the timescale of exchange within and between the conformational clusters; exchange must be on the millisecond to microsecond timescales to produce NMR broadening. However, the fact that both Y11D and Y11D HisH+ polypeptides adopt rare conformations not populated by the WT in the MC simulations suggests that one or more of these unique clusters are representative of the excited state detected by the NMR CPMG analysis. This idea is supported to some extent by the chemical shifts predicted for the unique MC clusters. In order for NMR broadening to occur, the chemical shifts of nuclei of interest must be different in the different states undergoing millisecond

timescale exchange. The observation of NMR broadening for residues throughout Y11D implies that the ^{15}N chemical shifts of the excited state are different than those of the ground state throughout the polypeptide chain. In qualitative agreement with the NMR results, the predicted chemical shifts of the MC clusters unique to Y11D are different from those of the ground state [Fig. 4(E,F)]. The differences are largest near the site of the Y > D substitution, but substantial differences are obtained for 15 residues or more toward the C-terminus. The agreement is not quantitative, as extensive spectral broadening is observed as far as position 34 by NMR, while the chemical shift difference found in MC calculations is more modest. Nevertheless, the computational prediction that the Y > D substitution leads the γ-CT to populate new conformations with distinct chemical shift patterns to a level of a few percent bears a striking similarity to what is observed by NMR.

Both NMR chemical shifts and MC simulations show that the yeast γ-tubulin CT polypeptide lacks persistent secondary or tertiary structure, that is, it is an intrinsically disordered region (IDR) domain. Intrinsically disordered proteins (IDPs) and IDRs are increasingly being recognized as a ubiquitous feature of the proteome with particular relevance to protein–protein interactions.[27] For example, the CTs of α- and β-tubulin are also IDRs that regulate microtubules via intermolecular interactions.[3,5,28] Local charge, for example the phosphorylation state of a residue within the IDR or the IDP, is frequently associated with the control of conformation and serves as a regulatory switch for protein–protein interactions and functionality.[29,30] In the case of the γ-CT polypeptide, a Y > D substitution at a known in vivo phosphorylation site causes it to undergo global cooperative transitions between different conformational states. Other intrinsically disordered protein domains have also been observed to undergo global cooperative conformational changes. In many cases, IDPs fold, that is, acquire regular secondary and higher order structure, upon interacting with a binding target.[31] Other IDP domains naturally exist in a dynamic equilibrium between disordered and ordered forms.[20] In an example of special relevance to this study, phosphorylation of the neuronal IDP 4E-BP2 causes it to fold into a four-stranded β-sheet and modulates its interactions with the el-F4E initiation factor.[29] What sets the Y11D γ-CT polypeptide apart from previous observations is that in other cases transitions occur between disordered and ordered states. Cooperativity in these examples, and protein folding in general, is believed to arise from specific steric requirements of forming a well-packed ordered structure containing long-range interactions.[32–34] In contrast, global concerted conformational transitions of the Y11D γ-CT occur between states that are entirely disordered. Long-range interactions are present, particularly, in more compact conformations (Supporting Information, Figs. S4 and S5). However, the γ-CT polypeptide lacks persistent secondary structure and specific, stable packing, or hydrogen bonding is absent. Thus, a Y11D substitution in a polypeptide corresponding to the γ-CT causes it to undergo a previously unreported type of protein motion involving collective transitions between two largely disordered conformational states. These results offer tantalizing clues as to how the post-translational modifications of the γ-CT contribute to its function in living cells. Preordering of unstructured peptides has been shown to modulate both the affinity and kinetics of binding to targets.[35,36] Phosphorylation of Tyr 11 could thus exert long-range effects on the kinetics and affinity of interactions targeting sites along the entire length of the γ-CT by modulating global conformational sampling.

The primary sequences of γ-CTs are distinct from the "E-hook" CTs of α- and β-tubulins, as γ-CTs contain stretches of hydrophobic residues interspersed with acidic (Asp, Glu) and polar residues. While both β-CTs and γ-CTs are intrinsically disordered, β-CTs carry higher net charge per residue comparing to γ-CTs and as result prediction of the conformational space of β-CTs suggests an extended ground state[8,9,26,28] relative to the more compact ground state of the γ-CT in our study. Previous studies suggest a combination of PTMs and residues specific to a given β-tubulin isoform controls a multitude of microtubule–MAP interactions with an extended and negatively charged β-CT[3–5]. In contrast for the γ-CT, PTMs such as phosphorylation could stimulate the transition from the more compact ground state to extended conformations, where charged and hydrophobic surfaces of the γ-CT are accessible. Intrinsically disordered regions of otherwise structured proteins frequently act to tune activity.[27] In a similar manner, control of conformational switching of the γ-CT may provide a tunable antenna for selective recruitment of proteins to γ-tubulin and as a consequence to new microtubules nucleated from γ-tubulin.

The idea that the γ-CT and specifically the Y11 phosphorylation state (Y445 in the full-length protein) serves as a tunable antennae for microtubule/MAP interactions is supported by our observations that an internal deletion of four residues (D443, S444, Y445, and L446) increases microtubule stability by altering the interaction between microtubule +ends and the microtubule tracking proteins EB1/Bim1 and Kar9; mutations that block the interaction between these proteins and the microtubules restore microtubule dynamical properties.[37] Furthermore, we recently found that the Y445D is correlated with partial collapse of the metaphase spindle, and is lethal when combined with mutations that disrupt

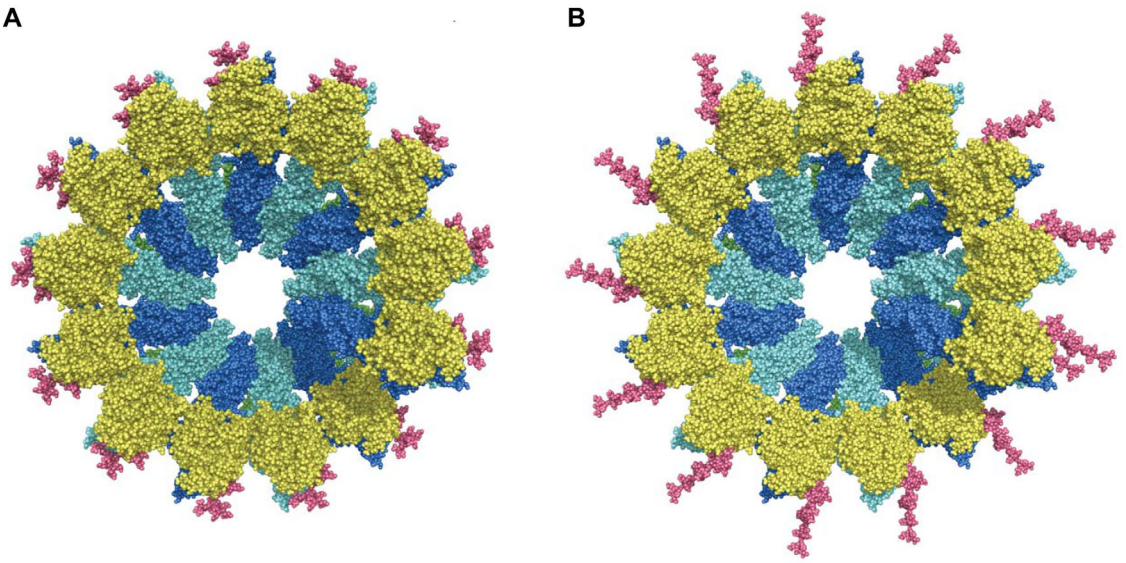

Figure 5. Visualization of the full γ-TURC with the compact (A) and extended (B) conformation of the γ-CT sampled during the MC simulations. Structure of the γ-TURC is taken from pdb 5FLZ. The compact and extended conformations of the γ-CT correspond to radii of gyration of 11.9 and 23.5 Å, respectively. Protein structures are shown as spheres. The γ-Tu, γ-CT, SPC97, SPC98, and SPC110 and are colored in gold, pink, cyan, blue, and light green, respectively.

cross-linked microtubules that maintain the stability of both metaphase and anaphase spindles.[38] This suggests that the phosphorylation state of Y445 may modulate the degree to which MAPs cross-link microtubules in the spindle. Deletion of the entire γ-CT (residues 444–475) has a profound effect on microtubule stability and the functions of the cytoplasmic microtubules and the mitotic spindle in living cells.[39]

We propose that the conformational sampling of the γ-CT is altered by the phosphorylation state of Y11 (Y445 in the full-length protein) and that this, in turn, modulates recruitment of MAPs, altering microtubule stability and function. The addition of negative charge via the Y11D substitution leads to increased sampling of extended conformations, likely in part due to increased electrostatic self-repulsion of the highly acidic polypeptide chain. The addition of a phosphate group at this position might be expected to have an even larger effect due to the greater negative charge (−1 for Y > D, −2 for Y > pY). To visualize the effects of altered conformational sampling of the γ-CT on MAP interactions, we have modeled it in a structural context more representative of the minus end of a microtubule. Two copies of full length γ-tubulin associate with the structural proteins SPC97 and SPC98 to form the heterotetrameric γ-tubulin small complex (γ-TUSC), which is stabilized by the N-terminal domain of SPC110.[40] The γ-TUSCs associate to form the γ-tubulin ring complex (γ-TURC), containing 13 γ-tubulins per turn, which is believed to nucleate microtubule formation.[40] In budding yeast cells, phosphorylation of Y445 occurs only in the pool of γ-tubulin bound to the spindle poles in the context of a γ-TURC.[7] We docked two simulated γ-CT structures, one drawn from the compact cluster 1 that is well populated by both WT and Y11D γ-CTs (R_g = 11.9 Å), and another from the extended cluster 25 that is exclusively populated by Y11D (R_g = 23.5 Å) (Supporting Information, Table S1 and Fig. S4) into the full γ-TURC to visualize the possible range of extension of γ-CT in relation to the rest of the complex (Fig. 5). The extended γ-CT [Fig. 5(B)] projects from the outer surface of the γ-TURC and is accessible relative to the collapsed γ-CT [Fig. 5(A)], with an exposed surface rich in non-polar and charged residues. A combination of hydrophobic and electrostatic interactions has been shown to be the basis of protein interactions with microtubules.[41] If Y445 phosphorylation is rare or occurs in a subpopulation of γ-TURCs (e.g., nuclear or cytoplasmic compartments), its combination with conformational switching of the γ-CT may regulate the interactions of individual microtubules with the diverse set of MAPs that endow microtubules with specific functions in the cell.

Materials and Methods

Protein production

The 35 C-terminal residues of S.c. γ-tubulin (γ-CT) were cloned into an His6 Sumo expression vector (Addgene plasmid #29711) with an SUMO domain and 6-histidine purification tag fused N-terminally, using standard techniques. ^{15}N and ^{15}N/^{13}C-enriched samples were prepared as follows:[42] *Escherichia coli* bacteria (BL21-DE3; EMD Biosciences, San Diego CA, USA) were transformed with the 6×His-SUMO-

γCT fusion plasmid. Bacteria were grown at 37°C in 4 L of LB broth to an OD_{600} 0.7, pelleted by centrifugation and resuspended in 1 L of M9 minimal media with $^{13}C/^{1}H$ glucose (Sigma-Aldrich, St. Louis MO, USA), and/or $^{15}NH_4Cl$ (Cambridge Isotope Laboratories, Andover MA, USA) as the sole sources of carbon and/or nitrogen. One hour after transfer to M9 medium, expression of 6×His-SUMO-γCT was induced with 200 mg isopropyl b-D-thiogalactoside (IPTG, Chem-Impex International Wood Dale IL, USA) and induction was allowed to proceed at 37°C. Bacteria were harvested after 6 h by centrifugation (4000 g 20 min). Cells were resuspended in a buffer containing 50mM potassium phosphate, 150mM potassium chloride, 1mM magnesium chloride, pH 7.5. The cells were disrupted by sonification and the insoluble material was separated by centrifugation (44,000 g 20 min). The SUMO-γCT was purified by using Toyoperl AF Chelate 350 His-tag affinity column (Tosoh bioscience, Montgomeryville PA, USA) and size exclusion chromatography using a HiLoad 16/60 Superdex 75 FPLC column (GE Healthcare, Little Chalfont, UK). The N-terminal 6xHis-SUMO tag was removed by incubation with 30μM SUMO protease (Ulp1, Addgene Sydney, Cambridge, USA) for 5 h at 30°C in 50 mM sodium phosphate, 100mM sodium chloride, pH 7.2, releasing a 39 residue γ-CT polypeptide (WT γ-CT: L L R G A A E Q D S **Y** L D D V L V D D E N M V G E L E E D L D A D G D H K L V; Y11D γ-CT: L L R G A A E Q D S **D** L D D V L V D D E N M V G E L E E D L D A D G D H K L V, in which Y11 corresponds to Y445 in the full protein). The γ-CT polypeptides were isolated by ion exchange chromatography using a HiTrap Q Sepharose FF FPLC column (GE Healthcare, Little Chalfont, UK). The γ-CT sample was then dialyzed against ddH_2O and 20 mM ammonium bicarbonate (ACP Chemicals Inc., Quebec, Canada). The solvent was removed via lyophilization. NMR samples (~1 mM) were prepared by dissolving the lyophilized powder in 50 mM sodium phosphate, 100 mM sodium chloride, 10% D_2O, 50 μM ethylene-diaminetetraacetic acid (EDTA, VWR West Chester PA, USA), 50 μM sodium azide (Sigma-Aldrich, St. Louis MO, USA) and the pH was adjusted to 6.5. 2,2-Dimethyl-2-silapentane-5-sulfonate (DSS, Sigma-Aldrich, St. Louis MO, USA, 0.35 mM) was used as an internal chemical shift reference.

NMR spectroscopy

NMR data for both WT and Y11D γ-CT polypeptides were recorded at 15°C using Varian INOVA spectrometers at ^{1}H Larmor frequencies of 500 MHz (11.7 T) and 800 MHz (18.8 T). The temperatures on both instruments were calibrated using a methanol reference.[43] Backbone assignments were obtained using $^{15}N/^{13}C$ labeled samples and HNCA, HNCO,[15] HNCACB,[16] CBCA(CO)NH,[17] C(CO)NH,[18] HCCONH,[18] and NOESY[44] experiments performed at 11.7 T. The data were processed using the NMRPipe/NMRDraw[45] suite of programs and analyzed using NMRView.[46] Residues (38 of 39) were assigned to 38 N–H correlations. A missing peak is attributed to the N-terminal residue. Several peaks in the Y11D γ-CT polypeptide could not be distinguished due to overlap of the peaks, and were therefore excluded from the backbone relaxation experiments.

Diffusion measurements

The self-diffusion coefficients (D_s) of the WT and Y11D γ-CT polypeptides were obtained at 11.7 T using an NMR PFG–water-sLED pulse sequence.[11] The gradient strengths were calibrated by using a 10% D_2O sample in a Shigemi tube (Shigemi Inc., Allison Park PA, USA). Data were acquired as arrays of 15 spectra (128 transients, 2 s recycle delay) with different gradient strengths (G_z) ranging from 1 to 30 G/cm. The ratio of intensities for a resonance with the gradient on (I) to that with the gradient off (I_0) is given by[11]

$$\frac{I}{I_0} = \exp\left[(-\gamma G_z \delta)^2 D_s \left(\Delta - {}^{\delta}/_{3}\right)\right] \quad (3)$$

where γ is the gyromagnetic ratio of ^{1}H (2.675×10^4 G^{-1} s^{-1}); G_z, and δ are the magnitude and duration of the gradient pulses, respectively; and Δ is the time between the gradient pulses. For our studies, the following parameters were used: $\delta = 2$ ms, $G_z = 1$–30 G/cm, $\Delta = 200$ ms, and a longitudinal eddy current delay of 2.0 ms. Diffusion coefficients were obtained from the slopes of plots of $\ln\{I/I_0\}$ versus G_z^2. The uncertainties in D_s were calculated as the standard deviations of values obtained from 5 methyl peaks that appeared in both wild-type and Y11D spectra.

Spin relaxation measurements

^{15}N R_1,[20] R_2,[21] and $R_{1\rho}$[47] relaxation rates were measured at 11.7 T. The R_1 experiments employed relaxation delays of 0.011, 0.089, 0.1779, 0.278, 0.400, 0.533, 0.667, and 0.889 s. The R_2 experiments employed relaxation delays of 0.01, 0.05, 0.09, 0.15, 0.21, 0.25, 0.35, and 0.45 s, during which refocusing pulses were applied every 1.2 ms (effective ν_{CPMG} field of ~400 Hz). The $R_{1\rho}$ experiments employed relaxation delays of 0.01, 0.02, 0.03, 0.04, 0.05, 0.06, 0.08, and 0.1 s and spin-lock field of 1.5–1.6 kHz. Relaxation rates were determined by nonlinear least-squares fitting of the peak intensities to the exponential decay function,

$$I(T_{relax}) = I_0 \cdot \exp(-RT_{relax}) \quad (4)$$

where T_{relax} is the delay time, I_0 is the initial peak intensity, and R is the relaxation rate.

Uncertainties in R_1, R_2, and $R_{1\rho}$ were estimated from the deviations between experimental peak intensities and their back-calculated values. R_2 values were calculated from experimental R_1 and $R_{1\rho}$ measurements according to the expression

$$R_{1\rho} = R_1 \cos^2\theta + R_2 \sin^2\theta \quad (5)$$

where

$$\theta = \tan^{-1}\left({}^{\nu_{SL}}/_{\Delta\nu}\right), \quad (6)$$

$\Delta\nu$ is the offset of the peak from the carrier frequency and ν_{SL} is the strength of the spin lock, in Hz. $\{^1H\}^{15}N$ steady-state NOE values were calculated as the ratio of peak volumes obtained with 5 s of proton presaturation and a 7 s interscan delay, relative to those obtained with no proton saturation and a 12 s interscan delay. Uncertainties were obtained from noise-level estimates in NMRDraw.[45]

CPMG measurements

^1H-decoupled ^{15}N Carr–Purcell–Meiboom–Gill (CPMG) experiments[23] with power compensation schemes[48] were performed with a 40 ms relaxation delay, 23 data points of ν_{CPMG} ranging from 25 to 1000 Hz, and ^1H decoupling fields of 12–13 kHz. Transverse relaxation rates, R_2, and their associated uncertainties, σ_{R2}, were calculated as described previously.[48] We fitted CPMG relaxation dispersion profiles using equations that describe conformational exchange between two states, A and B, associated with spin precession frequencies of ω_A and ω_B, and first-order rate constants k_{AB} and k_{BA}:

$$\omega_A \underset{k_{BA}}{\overset{k_{AB}}{\rightleftarrows}} \omega_B. \quad (7)$$

This can be parameterized in terms of the exchange rate, $k_{ex} = k_{AB} + k_{BA}$, the population of the minor (B) state, $p_B = k_{AB}/k_{ex}$, and the squared difference in precession frequency (or chemical shift) between the two states, $\Delta\omega^2 = (\omega_B - \omega_A)^2$. In the intermediate timescale regime, where $k_{ex} \approx |\Delta\omega|$, the transverse relaxation rate is given by[22]

$$R_2(\nu_{CPMG}) = \frac{1}{2}\left(R^0_{2,A} + R^0_{2,B} + k_{ex} - 2\nu_{CPMG}\cosh^{-1}(D_+\cosh(\eta_+) - D_-\cosh(\eta_-))\right)$$

$$D_\pm = \frac{1}{2}\left(\pm 1 + \frac{\psi + 2\Delta\omega^2}{\sqrt{\psi^2 + \xi^2}}\right)$$

$$\eta_\pm = \frac{\sqrt{2}}{4\nu_{CPMG}}\sqrt{\pm\psi + \sqrt{\psi^2 + \xi^2}}$$

$$\psi = \left(R^0_{2,A} - R^0_{2,B} + p_B k_{ex} - p_A k_{ex}\right)^2 - \Delta\omega^2 + 4 p_A p_B k_{ex}^2$$

$$\xi = 2\Delta\omega\left(R^0_{2,A} - R^0_{2,B} + p_B k_{ex} - p_A k_{ex}\right), \quad (8)$$

We fitted the relaxation dispersion profiles assuming that $R^0_{2A} = R^0_{2B}$. This is typically done in analyses of CPMG data, as it is not possible to reliably extract separate values for R^0_{2A} and R^0_{2B}.[49] This assumption is applicable to the Y11D γ-CT polypeptide as both states are disordered and thus likely have similar spin relaxation properties. Dispersion profiles were initially fitted by adjusting the values of k_{ex}, p_B, $\Delta\omega$, $R_2°$(500 MHz), and $R_2°$(800 MHz) on a per-residue basis to minimize the chi-squared function:

$$\chi^2 = \sum_i \frac{\left(\left(R_2^{calc}\right)_i - \left(R_2^{exp}\right)_i\right)^2}{\left(\sigma^2_{R2}\right)_i}, \quad (9)$$

where R_2^{calc} is calculated using Equation (8), and the sum runs over all R_2 values for a single residue at both 500 and 800 MHz for individual fits. CPMG data were then fit simultaneously such that one value of k_{ex} and one value of p_B were optimized globally while $\Delta\omega$, $R_2°$(500 MHz), and $R_2°$(800 MHz) were optimized on a per-residue basis to minimize χ^2, and the sum in Equation (9) runs over all residues at both 500 and 800 MHz. Uncertainties in the extracted parameters were estimated using a Monte Carlo approach in which the group fitting procedure was repeated for subsets of residues selected according to a bootstrap procedure.[50] Ten thousand bootstrap iterations were performed. The standard deviations of the k_{ex} and p_B estimates thus obtained were taken as the uncertainties in global k_{ex} and p_B values.

Monte Carlo simulations

Monte Carlo (MC) simulations on WT and Y11D γ-CTs were carried out by the CAMPARI package using the ABSINTH implicit solvation model and force-field paradigm[51] (http://campari.sourceforge.net/) with parameters adopted from the OPLS-AA (Optimized Potential for Liquid Simulations—All Atom) force field.[52] We considered two protonation states of His 36: neutral ε-protonated and positively charged ε,δ-protonated. In total, four different variants of γ-CT (WT, Y11D, WT HisH+, and Y11D HisH+) were computationally studied (Supporting Information, Fig. S2). The polypeptides were placed in spherical droplets of 75 A° radius and neutralized with Na^+ ions. Excess Na^+ and Cl^- ions were also added to the systems to mimic an ion concentration of 15 mM. A previous study[53] showed that the concentration of NaCl does not significantly affect the polymeric properties of the sampled conformational

ensembles but since ions are explicitly included in the MC simulations, adding a large number of ions results in high computational costs (see Supplementary Material for more information). The Van der Waals and electrostatic interactions between groups that are net neutral were cutoff at 10 and 14 Å, respectively. No cutoffs were used for electrostatic interactions involving ions and charged sidechains. The simulation temperature was also increased to 27°C to enhance conformational sampling. Conformational space for each polypeptide was sampled in 15 independent runs of 82,000,000 steps each using Markov Chain Metropolis Monte Carlo moves, where starting conformations of polypeptides and ion positions were randomly generated. The first 2,000,000 steps of each run were omitted, while the rest of trajectories were saved every 1,000 steps for the conformational analysis. In total, 1,200,000 conformations were used to calculate the polymeric properties of each polypeptide. A cluster analysis based on the positional RMSD of the Cartesian coordinates of Cα atoms was performed on every 10th conformation from the joined ensemble of both WT and Y11D γ-CTs as well as every 10th conformation from the joined ensemble of both WT HisH+ and Y11D HisH+ γ-CTs. Replicate cluster analysis calculations performed on different windows of 10 conformers from the joined ensembles (i.e., conformers 1,11,21,...; 2,12,22,...; 3,13,23,...; etc.) gave essentially identical results. A threshold radius of 10 A˚ was selected to define clusters. The SHIFTX program[54] was used to calculate ^{15}N chemical shifts of the backbone atoms of the sampled conformational ensembles. To estimate average diffusion coefficients, we calculated the diffusion coefficient for every 1000th conformation of the wild-type or mutant ensembles using the HydroNMR7 program[55] and found their mean values. Parameters for diffusion coefficient calculations were adopted from Mao et al.[26] The polypeptide conformations were visualized in the VMD software.[56] All calculations were performed on a CentOS 5 Calcul Québec high-performance computational cluster.

Other details of the simulation setup—including move sets used, choice for droplet size, number of replicate simulations, and number of steps—are provided in Supporting Information. A structure of the full γ-TURC (pdb 5FLZ) was used for visualization of the ring complex with the compact and extended conformations of the γ-CT. The compact and extended conformations of the γ-CT were selected from clusters 1 and 25, respectively, with neutral His 36. The visualization was performed in Discovery Studio Visualizer.[57]

Acknowledgments

The authors thank members of the Mittermaier and Vogel labs for many helpful discussions, and Mickaela Nixon and Conrad Hall for γ-CT cloning and initial expression experiments. The authors declare no competing interests.

References

1. Nogales E, Wolf SG, Downing KH (1998) Structure of the alpha beta tubulin dimer by electron crystallography. Nature 391:199–203.
2. Aldaz H, Rice LM, Stearns T, Agard DA (2005) Insights into microtubule nucleation from the crystal structure of human gamma-tubulin. Nature 435:523–527.
3. Janke C (2014) The tubulin code: molecular components, readout mechanisms, and functions. J Cell Biol 206:461–472.
4. Wehenkel A, Janke C (2014) Towards elucidating the tubulin code. Nat Cell Biol 16:303–305.
5. Sirajuddin M, Rice LM, Vale RD (2014) Regulation of microtubule motors by tubulin isotypes and post-translational modifications. Nat Cell Biol 16:335–344.
6. Vogel J, Drapkin B, Oomen J, Beach D, Bloom K, Snyder M (2001) Phosphorylation of gamma-tubulin regulates microtubule organization in budding yeast. Dev Cell 1:621–631.
7. Keck JM, Jones MH, Wong CC, Binkley J, Chen D, Jaspersen SL, Holinger EP, Xu T, Niepel M, Rout MP, Vogel J, Sidow A, Yates JR, 3rd, Winey M (2011) A cell cycle phosphoproteome of the yeast centrosome. Science 332:1557–1561.
8. Luchko T, Huzil JT, Stepanova M, Tuszynski J (2008) Conformational analysis of the carboxy-terminal tails of human beta-tubulin isotypes. Biophys J 94:1971–1982.
9. Freedman H, Luchko T, Luduena RF, Tuszynski JA (2011) Molecular dynamics modeling of tubulin C-terminal tail interactions with the microtubule surface. Proteins 79:2968–2982.
10. Martin EW, Holehouse AS, Grace CR, Hughes A, Pappu RV, Mittag T (2016) Sequence determinants of the conformational properties of an intrinsically disordered protein prior to and upon multisite phosphorylation. J Am Chem Soc 138:15323–15335.
11. Altieri AS, Hinton DP, Byrd RA (1995) Association of biomolecular systems via pulsed field gradient NMR self-diffusion measurements. J Am Chem Soc 117: 7566–7567.
12. Zhou H (2002) Dimensions of denatured protein chains from hydrodynamic data. J Phys Chem B 106:5769–5775.
13. Wilkins DK, Grimshaw SB, Receveur V, Dobson CM, Jones JA, Smith LJ (1999) Hydrodynamic radii of native and denatured proteins measured by pulse field gradient NMR techniques. Biochemistry 38:16424–16431.
14. Kragelj J, Ozenne V, Blackledge M, Jensen MR (2013) Conformational propensities of intrinsically disordered proteins from NMR chemical shifts. ChemPhysChem 14:3034–3045.
15. Ikura M, Kay LE, Bax A (1990) A novel approach for sequential assignment of proton, carbon-13, and nitrogen-15 spectra of larger proteins: heteronuclear triple-resonance three-dimensional NMR spectroscopy. Application to calmodulin. Biochemistry 29:4659–4667.
16. Wittekind M, Mueller L (1993) HNCACB, a high-sensitivity 3D NMR experiment to correlate amide-proton and nitrogen resonances with the alpha- and

beta-carbon resonances in proteins. J Magn Reson B 101:201–205.
17. Grzesiek S, Bax A (1992) Correlating backbone amide and side chain resonances in larger proteins by multiple relayed triple resonance NMR. J Am Chem Soc 114:6291–6293.
18. Grzesiek S, Anglister J, Bax A (1993) Correlation of backbone amide and aliphatic side-chain resonances in 13C/15N-enriched proteins by isotropic mixing of 13C magnetization. J Magn Reson B 101:114–119.
19. Camilloni C, De Simone A, Vranken WF, Vendruscolo M (2012) Determination of secondary structure populations in disordered states of proteins using nuclear magnetic resonance chemical shifts. Biochemistry 51: 2224–2231.
20. Farrow N, Zhang O, Forman-Kay J, Kay L (1994) A heteronuclear correlation experiment for simultaneous determination of 15N longitudinal decay and chemical exchange rates of systems in slow equilibrium. J Biomol NMR 4:727–734.
21. Kay LE, Torchia DA, Bax A (1989) Backbone dynamics of proteins as studied by N-15 inverse detected heteronuclear NMR spectroscopy - application to staphylococcal nuclease. Biochemistry 28:8972–8979.
22. Palmer AG, Kroenke CD, Loria JP (2001) Nuclear magnetic resonance methods for quantifying microsecond-to-millisecond motions in biological macromolecules. Methods Enzymol 339:204–238.
23. Hansen DF, Vallurupalli P, Kay LE (2008) An improved (15)N relaxation dispersion experiment for the measurement of millisecond time-scale dynamics in proteins. J Phys Chem B 112:5898–5904.
24. Kovrigin EL, Kempf JG, Grey MJ, Loria JP (2006) Faithful estimation of dynamics parameters from CPMG relaxation dispersion measurements. J Magn Reson 180:93–104.
25. Millet O, Loria JP, Kroenke CD, Pons M, Palmer AG (2000) The static magnetic field dependence of chemical exchange linebroadening defines the NMR chemical shift time scale. J Am Chem Soc 122:2867–2877.
26. Mao AH, Crick SL, Vitalis A, Chicoine CL, Pappu RV (2010) Net charge per residue modulates conformational ensembles of intrinsically disordered proteins. Proc Natl Acad Sci USA 107:8183–8188.
27. Wright PE, Dyson HJ (2015) Intrinsically disordered proteins in cellular signalling and regulation. Nat Rev Mol Cell Biol 16:18–29.
28. Roll-Mecak A (2015) Intrinsically disordered tubulin tails: complex tuners of microtubule functions?. Semin Cell Dev Biol 37:11–19.
29. Bah A, Vernon RM, Siddiqui Z, Krzeminski M, Muhandiram R, Zhao C, Sonenberg N, Kay LE, Forman-Kay JD (2015) Folding of an intrinsically disordered protein by phosphorylation as a regulatory switch. Nature 519:106–109.
30. Travers T, Shao H, Joughin BA, Lauffenburger DA, Wells A, Camacho CJ (2015) Tandem phosphorylation within an intrinsically disordered region regulates ACTN4 function. Sci Signal 8:ra51.
31. Sugase K, Dyson HJ, Wright PE (2007) Mechanism of coupled folding and binding of an intrinsically disordered protein. Nature 447:1021–U1011.
32. Abkevich VI, Gutin AM, Shakhnovich EI (1995) Impact of local and nonlocal interactions on thermodynamics and kinetics of protein-folding. J Mol Biol 252: 460–471.
33. Kolinski A, Galazka W, Skolnick J (1996) On the origin of the cooperativity of protein folding: implications from model simulations. Proteins 26:271–287.
34. Chan HS, Shimizu S, Kaya H, Cooperativity principles in protein folding. In: Holt JM, Johnson ML, Ackers GK, Eds. (2004) Energetics of biological macromolecules, part E. Elsevier, pp 350–379.
35. Ferreon JC, Hilser VJ (2003) The effect of the polyproline II (PPII) conformation on the denatured state entropy. Protein Sci 12:447–457.
36. Ferreon JC, Hilser VJ (2004) Thermodynamics of binding to SH3 domains: the energetic impact of polyproline II (PII) helix formation. Biochemistry 43:7787–7797.
37. Cuschieri L, Miller R, Vogel J (2006) Gamma-tubulin is required for proper recruitment and assembly of Kar9-Bim1 complexes in budding yeast. Mol Biol Cell 17: 4420–4434.
38. Shulist K, Yen E, Kaitna S, Leary A, Decterov A, Gupta D, Vogel J (2017) Interrogation of gamma-tubulin alleles using high-resolution fitness measurements reveals a distinct cytoplasmic function in spindle alignment. Sci Rep 7:11398.
39. Vogel J, Snyder M (2000) The carboxy terminus of Tub4p is required for gamma-tubulin function in budding yeast. J Cell Sci 113: 3871–3882.
40. Kollman JM, Greenberg CH, Li S, Moritz M, Zelter A, Fong KK, Fernandez JJ, Sali A, Kilmartin J, Davis TN, Agard DA (2015) Ring closure activates yeast gammaTuRC for species-specific microtubule nucleation. Nat Struct Mol Biol 22:132–137.
41. Akhmanova A, Steinmetz MO (2015) Control of microtubule organization and dynamics: two ends in the limelight. Nat Rev Mol Cell Biol 16:711–726.
42. Marley J, Lu M, Bracken C (2001) A method for efficient isotopic labeling of recombinant proteins. J Biomol NMR 20:71–75.
43. Ammann C, Meier P, Merbach A (1982) A simple multinuclear NMR thermometer. J Magn Reson 46:319–321.
44. Zhang O, Kay L, Olivier JP, Forman-Kay J (1994) Backbone 1H and 15N resonance assignments of the N-terminal SH3 domain of drk in folded and unfolded states using enhanced-sensitivity pulsed field gradient NMR techniques. J Biomol NMR 4:845–858.
45. Delaglio F, Grzesiek S, Vuister G, Zhu G, Pfeifer J, Bax A (1995) NMRPipe: a multidimensional spectral processing system based on UNIX pipes. J Biomol NMR 6:277–293.
46. Johnson BA (2004) Using NMRView to visualize and analyze the NMR spectra of macromolecules. Methods Mol Biol 278:313–352.
47. Baldwin A, Kay L (2013) An R1ρ expression for a spin in chemical exchange between two sites with unequal transverse relaxation rates. J Biomol NMR 55:211–218.
48. Demers J-P, Mittermaier A (2009) Binding mechanism of an SH3 domain studied by NMR and ITC. J Am Chem Soc 131:4355–4367.
49. Ishima R, Torchia DA (2006) Accuracy of optimized chemical-exchange parameters derived by fitting CPMG R-2 dispersion profiles when R-2(0a) = R-2(0b). J Biomol NMR 34:209–219.
50. Efron B, Tibshirani R (1986) Bootstrap methods for standard errors, confidence intervals, and other measures of statistical accuracy. Stat Sci 1:54–77.
51. Vitalis A, Pappu RV (2009) ABSINTH: a new continuum solvation model for simulations of polypeptides in aqueous solutions. J Comput Chem 30:673–699.
52. Kaminski GA, Friesner RA, Tirado-Rives J, Jorgensen WL (2001) Evaluation and reparametrization of the OPLS-AA force field for proteins via comparison with

accurate quantum chemical calculations on peptides. J Phys Chem B 105:6474–6487.
53. Das RK, Pappu RV (2013) Conformations of intrinsically disordered proteins are influenced by linear sequence distributions of oppositely charged residues. Proc Natl Acad Sci USA 110:13392–13397.
54. Neal S, Nip AM, Zhang H, Wishart DS (2003) Rapid and accurate calculation of protein 1H, 13C and 15N chemical shifts. J Biomol NMR 26:215–240.
55. Garcia de la Torre J, Huertas ML, Carrasco B (2000) HYDRONMR: prediction of NMR relaxation of globular proteins from atomic-level structures and hydrodynamic calculations. J Magn Reson 147: 138–146.
56. Humphrey W, Dalke A, Schulten K (1996) VMD: visual molecular dynamics. J Mol Graph 14:33–38.
57. Dassault Systèmes BIOVIA (2015) Discovery studio visualizer, v16.1.0.15350. San Diego: Dassault Systèmes.